11.2 POLARIMETRIC RADAR CHARACTERISTICS OF LARGE HAIL

Matthew R. Kumjian*[1,2,3,4], Joseph C. Picca[1,2,3,4], Scott M. Ganson[3], Alexander V. Ryzhkov[1,2,4], John Krause[1,2], Dušan Zrnić[2], and Alexander Khain[5]

1. Cooperative Institute for Mesoscale Meteorological Studies, Norman, OK
2. National Severe Storms Laboratory, Norman, OK
3. School of Meteorology, University of Oklahoma, Norman, OK
4. Atmospheric Radar Research Center, Norman, OK
5. Hebrew University of Jerusalem, Givat Ram, Jerusalem, Israel

1. INTRODUCTION

The advantage of dual-polarization radar data in the discrimination of precipitation types has been demonstrated successfully (e.g., Straka et al. 2000; Liu and Chandrasekar 2001; Lim et al. 2005; Park et al. 2009; Clabo et al. 2009), including the detection of hail among other precipitation echoes (e.g., Wakimoto and Bringi 1988; Heinselman and Ryzhkov et al. 2006; Depue et al. 2007). Conventional detection of hail using dual-polarization data is based on the idea that large hail tumbles as it falls, leading to differential reflectivity (Z_{DR}) near 0 dB. Regions of a storm that have large reflectivity factor (Z_H) and near-zero Z_{DR} are then assumed to contain hail. Additionally, when the radar probing volume is filled with a mixture of hydrometeor types (e.g., rain and hail), the measured copolar cross-correlation coefficient (ρ_{HV}) will be decreased.

The problem with the conventional method described above is its oversimplification. The melting process leads to nonuniform scattering characteristics of hailstones across the size spectrum; these differences significantly affect the measured polarimetric variables. Details of the melting process, as well as other factors (such as fall behavior and particle axis ratio) that affect the scattering characteristics of hailstones are provided in the next section.

Despite the general success of detecting the presence of hail with polarimetric radar, of utmost importance for operational meteorologists is the detection of *severe* or "large" hail, defined by the U.S National Weather Service as having a diameter > 2.5 cm (1.0"). This paper investigates the polarimetric radar properties of hailstones across the size spectrum in order to develop a method of discriminating between large and small hail, which will allow meteorologists to better detect potentially damaging hailstorms. Previous attempts at such discrimination (Liu and Chandrasekar 2001; Lim et al. 2005; Depue et al. 2007) have had mixed success, and none has explicitly considered the melting process. In fact, Liu and Chadrasekar (2001) and Lim et al. (2005) do not define what is meant by "large" and "small" hail. To alleviate such confusion, we will use the following definitions: large hail refers to equivolume diameters in excess of 2.5 cm, and "giant" hail refers to those stones with diameters exceeding 5.0 cm (2.0").

This paper will be structured as follows. In section 2, an overview is given of various factors affecting scattering properties of hailstones that must be taken into consideration when developing discrimination rules. Section 3 presents the theoretical approach to determining the polarimetric characteristics of large hail, beginning with idealized computations based on scattering theory and working towards increased complexity with the use of two theoretical models. The fourth section presents polarimetric radar observations made in cases with and without reported large hail. A synthesis of the results in Section 5 culminates in a novel set of rules used to discriminate between small and large hail. The results and caveats are summarized briefly in section 6.

2. FACTORS AFFECTING SCATTERING PROPERTIES

2.1. Melting

As a hailstone descends beneath the melting layer, the acquisition of liquid meltwater significantly affects its scattering properties. Importantly, the *distribution* of that meltwater makes a substantial difference in the measured polarimetric variables: liquid water can be absorbed into cavities within the particle ("spongy ice"), collected on the outside of the particle as a water "coating," and sometimes shed as liquid drops (e.g., Rasmussen and Heymsfeld 1987; herein RH87). How the liquid water is distributed in the particle is based (in part) on its size. For example, smaller melting hailstones tend to acquire a substantial liquid water coat, whereas larger stones shed excess meltwater (RH87). The degree of melting is a function of how far the hailstones have descended below the 0 °C wetbulb temperature level. Therefore, any discrimination efforts

**Corresponding Author:* Matthew R. Kumjian, 120 David L. Boren Blvd., NWC Suite 4900, Norman, OK 73072. E-mail: matthew.kumjian@noaa.gov

should incorporate information about the melting layer height.

2.2 Fall behavior

Another factor significantly affecting the radar observations of hailstones is fall behavior. Spherical particles may tumble as they fall; however, their fall behavior is irrelevant as scattering is isotropic for spherical particles. Regarding nonspherical particles, most previous studies have concluded that the preferred fall mode of such stones is symmetric gyration (e.g., Knight and Knight 1970; Kry and List 1974; see also a review by Böhm 1991 and references therein). Specifically, hailstones tend to spin about their minor axes (which trace out a cone symmetric about the horizontal plane through the center of the spheroid), with their total angular momentum in the horizontal (Kry and List 1974). Indeed, as will be shown later, observed nonzero Z_{DR} values in dry hail suggests that these particles have some degree of orientation, not random tumbling. Orientation may be enhanced in convective storm updrafts, where hailstones are kept at a near-constant altitude as they are advected horizontally (e.g., Nelson 1983). Better alignment of giant (> 5 cm) oblate hailstones in the updraft may be the reason for more frequent observations of polarimetric three-body scatter signatures aloft emanating from cores with substantial negative Z_{DR} (Kumjian et al. 2010a).

2.3 Axis Ratios

The axis ratio of hailstones has a substantial impact on the resulting polarimetric variables. Knight (1986) observed hailstones collected from the ground and found that stones become less spherical with increasing diameter from small to large sizes, then approximately level off for sizes greater than about 2.5 cm (Fig. 1). Knight (1986) suggests that based on the small number of samples available for stones exceeding 6 cm in diameter, there is a trend for shapes to be more spherical due to the significant tumbling of such giant stones. The calculations herein will be based on Knight's measurements.

3. THEORETICAL APPROACH

Because of the different factors contributing to uncertainty, our theoretical approach will work upscale, starting from computations of individual particles and gradually adding levels of complexity.

3.1 T-matrix for individual particles

A T-matrix code is used to compute complex scattering amplitudes for individual particles, from which the polarimetric radar variables are calculated following Ryzhkov (2001). First we will consider dry

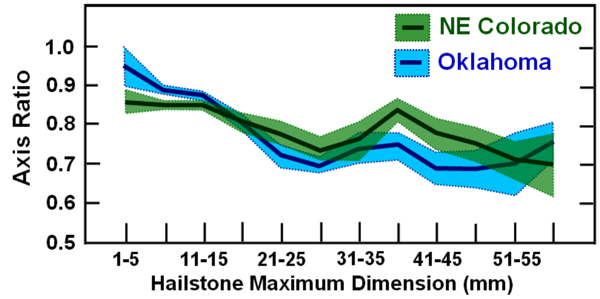

Fig. 1: Hailstone axis ratio as a function of its maximum dimension. Colored envelopes represent the 95% confidence interval. Data are based on 2675 samples collected in northeastern Colorado (green) and 1790 samples from Oklahoma (blue). Adapted from Knight (1986).

hailstones, before the onset of melting (Fig. 2a). Our results are in very good agreement with previous studies (e.g., Aydin and Zhao 1990; Balakrishnan and Zrnić 1990). Note that the Z_{DR} for the oblate dry hailstones is positive until the size reaches about 5.5 cm, with a peak for sizes between 4 and 5 cm. This first peak is a resonance at horizontal (H) polarization, which causes the backscattered power at H polarization to increase dramatically over the backscattered power at vertical (V) polarization. For larger sizes (> 5.5 cm), Z_{DR} becomes strongly negative. This minimum in Z_{DR} is due to the resonance at V-polarization as the H-polarization resonance is passed (i.e., the backscattered power at V polarization becomes stronger than that at H polarization). Therefore, large *oblate* dry hailstones can have both positive and *negative* Z_{DR} at S band. An increase in the rms width of the canting angle distribution (σ) tends to dampen the Z_{DR} extremes.

To crudely approximate the effect of melting, the same computations are reproduced for hailstones with a thin (0.5-mm) water coat (Fig. 2b). A uniform water coat across the size spectrum is oversimplified; a more rigorous treatment should include a physical model of the melting process, which is described in the next subsection. Owing to the increased dielectric of the particles because of the presence of liquid water, the first positive maximum (first resonance at H-polarization) occurs for smaller sizes, between 3 and 4 cm. This maximum in Z_{DR} is also larger than for the dry hailstone case. The minimum in Z_{DR} (negative values) also occurs for smaller sizes and is significantly decreased in magnitude.

The differential phase shift upon backscatter (δ) is the argument of ρ_{HV} in the absence of propagation effects. Nonzero values of δ are a by-product of resonance (non-Rayleigh) scattering in anisotropic particles. A large diversity of δ within the sampling volume will cause a considerable decrease in the measured ρ_{HV}. Hailstones of the particular band of sizes where δ undergoes large variations will then contribute to a decreased ρ_{HV}. These oscillations in δ

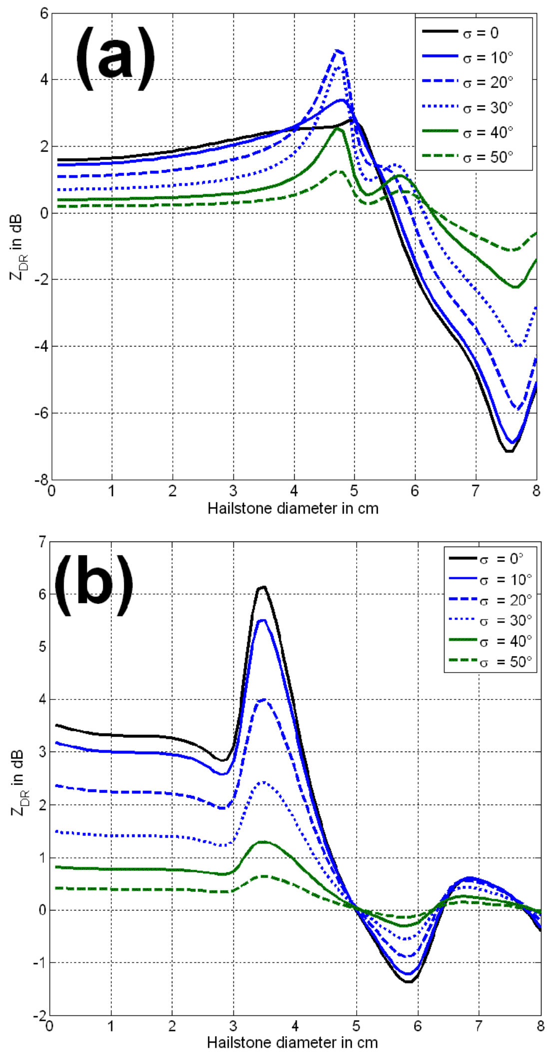

Fig. 2: (a) T-matrix computations of Z_{DR} (at S band) as a function of size for dry, oblate hailstones (axis ratio a/b = 0.7). Each curve represents a different rms width of the canting angle distribution (σ). (b) As in (a), except for hailstones with a 0.5-mm water coat.

occur for the same sizes as the extrema in the Z_{DR} curves (Fig. 3). As with Z_{DR}, more chaotic orientation decreases δ. In storms, hail size distributions that contain the band of "resonance scatterers" will lead to decreased ρ_{HV}, even for dry stones aloft at subfreezing temperatures. Additionally, surface irregularities on hailstones such as lobes or spikes can substantially lower the observed ρ_{HV} (e.g., Balakrishnan and Zrnić 1990).

3.2 Melting Hail Model

The first microphysics model we will use is the one-dimensional explicit microphysics model of melting hail, which is described in Ryzhkov et al. (2009), Ryzhkov et al. (2010), and Kumjian and Ryzhkov (2008a). The model is based on the RH87

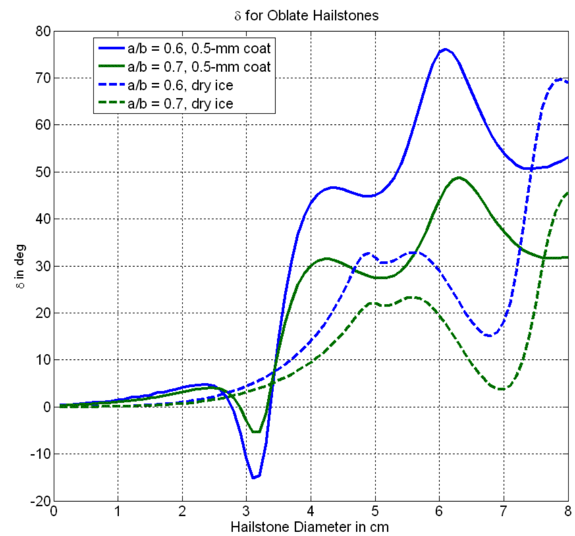

Fig. 3: Backscatter differential phase (δ) for oblate hailstones (a/b = 0.6, blue lines, a/b = 0.7 for green lines). Computations are shown for both dry stones (dashed curves) and 0.5-mm water coated stones (solid curves) that are oriented with their minor axis in the vertical with σ = 0°.

melting study and accounts for melting and shedding of hailstones of diameters 0.1 mm to 4.0 cm, but does not account for particle interactions. Vertical profiles of the polarimetric variables are computed using a T-Matrix code, assuming spongy hail.

The model is capable of reproducing realistic vertical profiles of polarimetric variables at S and C bands, including the differences between signatures at S and C bands (Fig. 4). These modeling results clearly show that the height of the radar sampling volume relative to the melting layer is of crucial importance for any discrimination efforts. Importantly, Ryzhkov et al. (2009) found that hailstones larger than about 2.5 cm – 3.0 cm (i.e., "large hail" by our definition) contribute very little to all polarimetric variables using their assumed size distributions; in contrast, small melting hail (0.57 – 2.0 cm) has the largest impact on the polarimetric variables except K_{DP} (Fig. 5).

Another important consideration regarding the melting process is the distribution of liquid water in the hailstone as it melts. Generally, two models are used to describe the distribution of meltwater: the first is spongy ice, where the density of the hailstone is less than that of solid ice (< 917 kg m^{-3}) and meltwater first fills the air pockets inside the stone; secondly, the hailstone has the density of solid ice, and all meltwater collects on the outside of the stone. In electromagnetic models, the spongy ice model is addressed using a mixture formula, wherein the dielectric of the melting hailstone is treated as a uniform mixture of water and ice, whereas a two-layer model is used for the case of

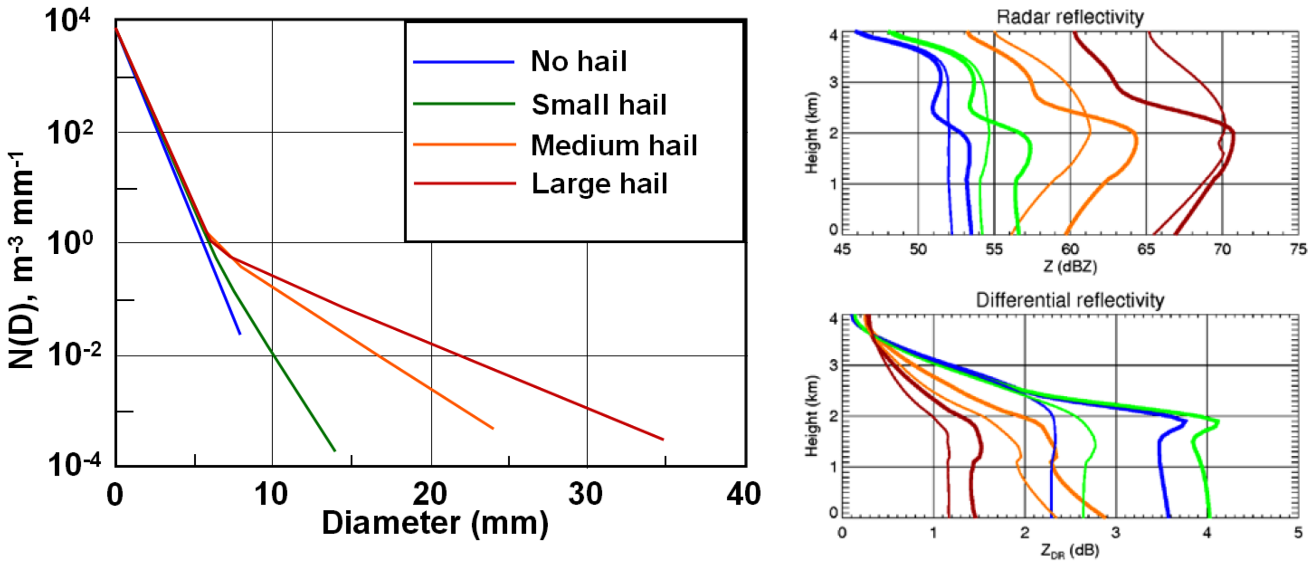

Fig. 4: Particle size distributions used in the simulations (left panel). Vertical profiles of Z_H (top, right panel) and Z_{DR} (bottom, right panel). Thick curves are for C band, thin curves are for S band. Adapted from Ryzhkov et al. (2009).

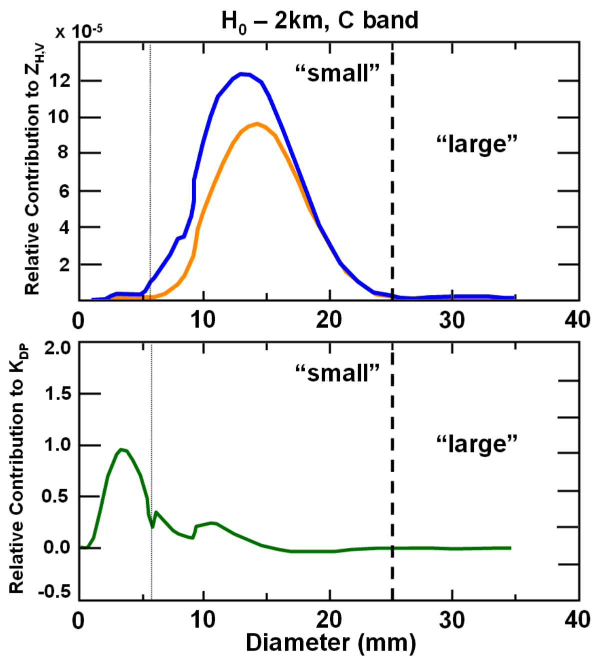

Fig. 5: Relative contributions to Z_H and Z_V (top panel, blue and orange curves, respectively) and K_{DP} (bottom panel) from melting hailstones with equivalent volume diameters as indicated on the abscissa. The units of the ordinate axes are arbitrary. The vertical dashed line separates "small" and "large" hail. The thin dotted vertical line separates particles that have totally melted to raindrops on the left, and those particles with ice cores on the right. From the microphysics model at 2 km below the melting level H_0, at C band. Adapted from Ryzhkov et al. (2009).

water coating a solid ice core (e.g., see Ryzhkov et al. 2010).

The difference in scattering between the "spongy" and "coated" hailstones can be striking. Figs. 6 – 7 are computed Z_H and Z_{DR} values for spongy and coated hailstones, respectively. Notably, there is a nearly 20 dBZ difference between Z_H values for large (> 25 mm) hail at S and C bands, and an even larger difference between S and X bands. In general, Z_H values are larger for the spongy model than for the water-coated model. In Fig. 7, the most notable difference between spongy and coated hailstones is the oscillation for spongy hail at C band at about 25 mm. Whereas the coated model provides mainly positive Z_{DR} values for all wavelengths, the C-band curve drops to nearly -3 dB in the spongy model. It is clear that the distribution of meltwater significantly impacts the electromagnetic response of the radar signal.

3.3 The Hebrew University Cloud Model

The Hebrew University Cloud Model (HUCM; see Khain et al. 2004) is used next to account for more realistic in-cloud conditions. The model is an explicit microphysics bin model, which contains 43 mass-doubling particle size bins. Such a bin model allows for a more sophisticated treatment of microphysics, including all sorts of particle interactions and more realistic particle size distributions. The main limitation of the HUCM is that it is two-dimensional; thus, three-dimensional features (such as mesocyclones) that are important for the growth of giant hail cannot be simulated.

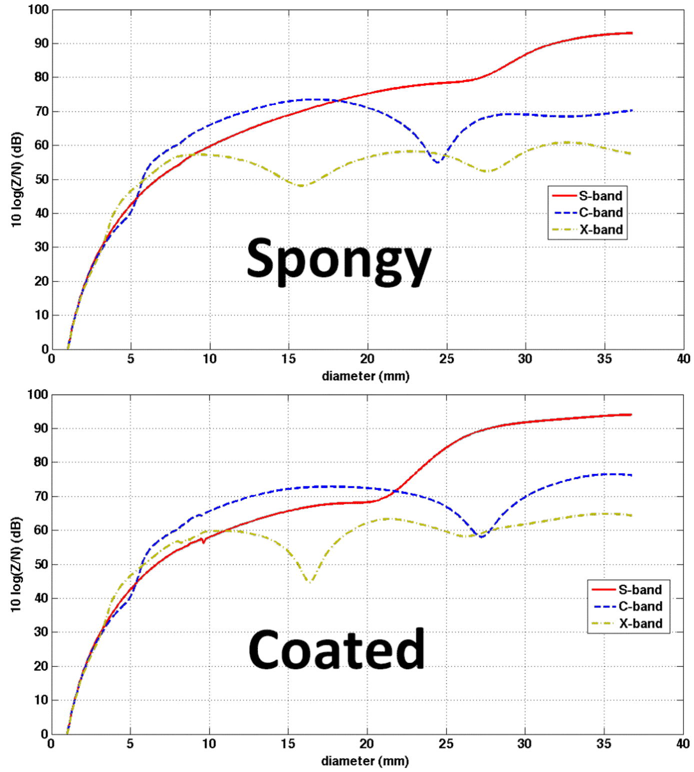

Fig. 6: Z_H values for spongy hail (top panel) and water-coated hail (bottom panel) as a function of diameter for three radar wavelengths. Meltwater fractions are computed from the 1-D melting hail model 4 km below the environmental freezing level.

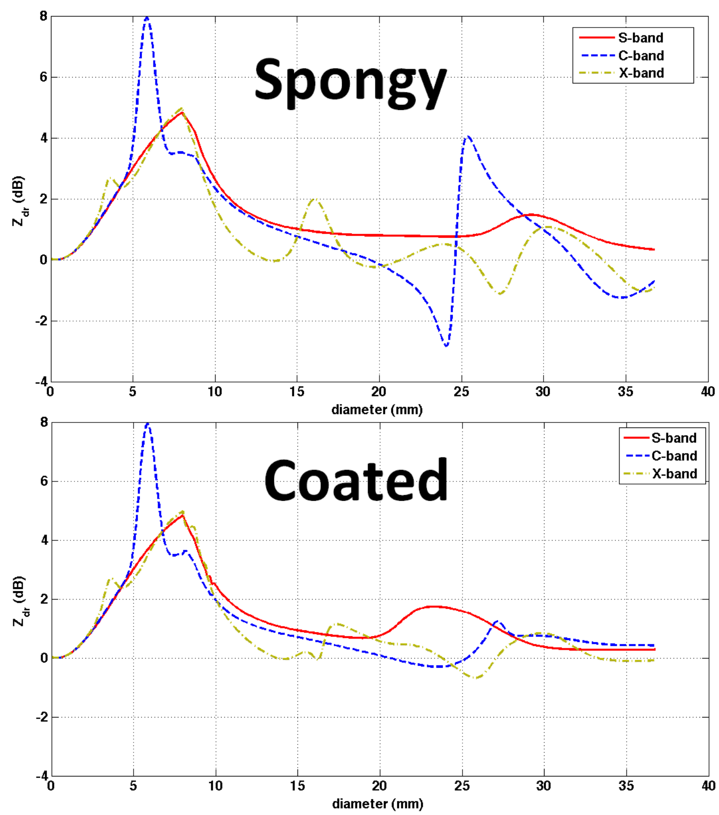

Fig. 7: As in Fig. 6, except Z_{DR} is shown.

The storm simulated is the one described in Ryzhkov et al. (2010), which produces large hail. To quantify the amount of large hail, the output from the HUCM is converted to mass, and the mass particle size bins for hail larger than 2.5 cm (1") were summed to obtain what we call the *large hail mass* (LHM). A certain LHM threshold was selected to exclude from statistics the model grid cells with very small (practically insignificant) LHM. The minimum threshold was chosen quasi-subjectively based on the large hail total concentration: one hailstone per grid cell in the model (0.35 x 0.15 km). This threshold is equivalent to assuming a minimum total number concentration of large hail of 10^{-5} m^{-3}, which is consistent with similar definition (expressed via hail flux) of Milbrandt and Yau (2006). Similar to large hail mass, the *small hail mass* (SHM) was determined as the total mass of hailstones with sizes between 1.0 and 2.5 cm.

Several hours into the simulation, a mature hail-bearing storm is produced. Z_H and Z_{DR} are computed from the output particle size distributions for each model grid cell following Ryzhkov et al. (2010). Using the computed polarimetric radar variables and the distributions of LHM and SHM, two-dimensional frequency distributions for Z_H and Z_{DR} occurrence in grid cells that contain appreciable LHM and SHM are constructed for different height intervals (Fig. 8). Note that the environmental freezing level is at 2.5 km AGL. The retrievals illustrate differences between the polarimetric characteristics of areas within the storm containing small and large hail; these differences are especially pronounced at lower levels. The HUCM cloud model retrievals confirm the results from the more simplistic one-dimensional melting hail model, increasing confidence in our computations and inferences.

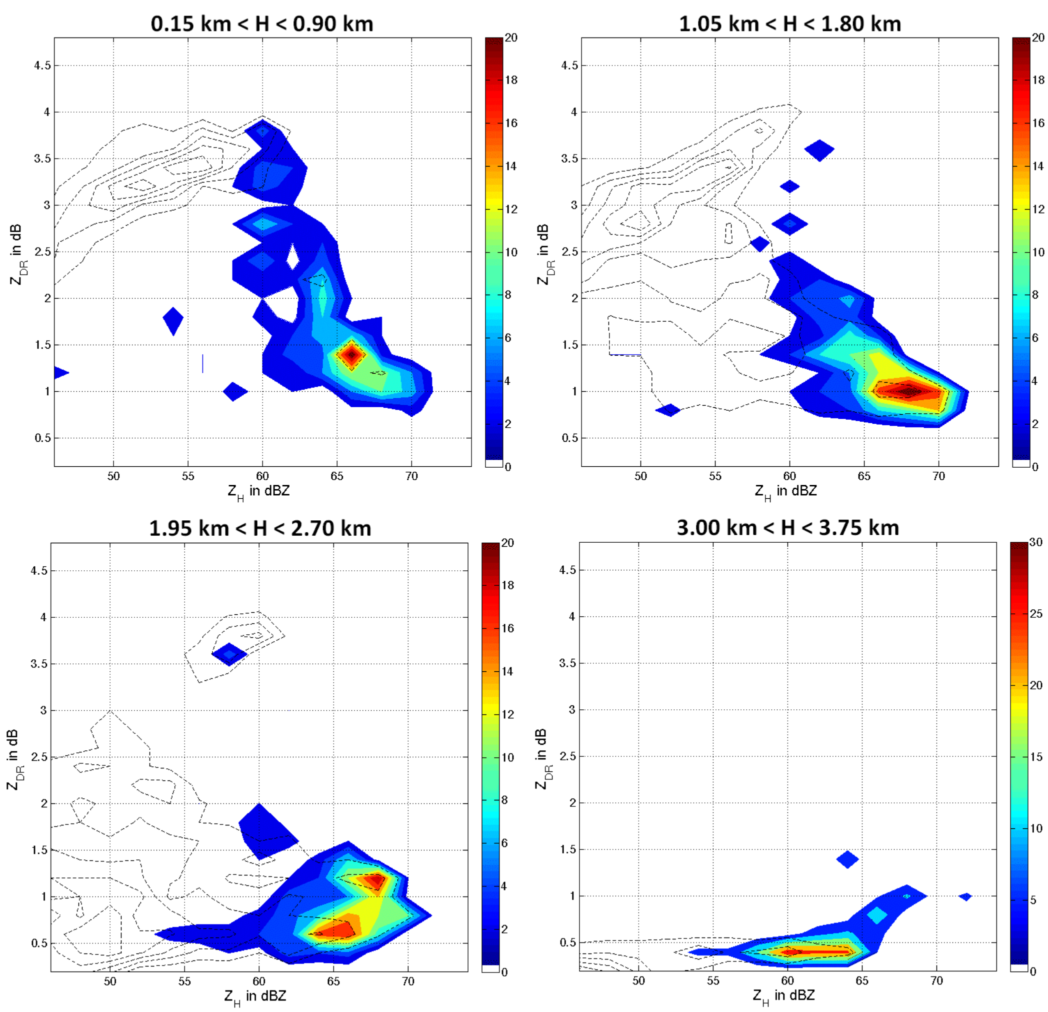

Fig. 8: Frequency distributions of LHM (shading) and SHM (dashed contours) as a function of Z_H and Z_{DR}, based on output from the HUCM. The title above each panel indicates the height interval (AGL) from which the distributions are computed. The environmental freezing level is at 2.5 km.

Contributions to Z_H from rain are dominant for most regions of the storm at low levels (Fig. 9), except for between x = 102 km – 104 km, where the contributions from hail result in significantly higher total Z_H (70 dBZ, compared to 40-60 dBZ for rain only). The total Z_{DR} reflects the Z_{DR} contributions from rain at almost every point except in the large hail core, where total Z_{DR} is lowered substantially. However, there are large Z_{DR} values located to the east (at about x = 104 km) of the maximum in LHM, which are attributed to rain and not melting hail. This implies that Z_{DR} may be positive in regions with large hail if collocated with large enough concentrations of raindrops. Resonance scattering effects at C band are likely to contribute even more strongly to positive Z_{DR} when raindrops and large hail are collocated within the sampling volume. Also of note is that appreciable LHM (above the thresholded value) is present for Z_H as low as about 40 dBZ.

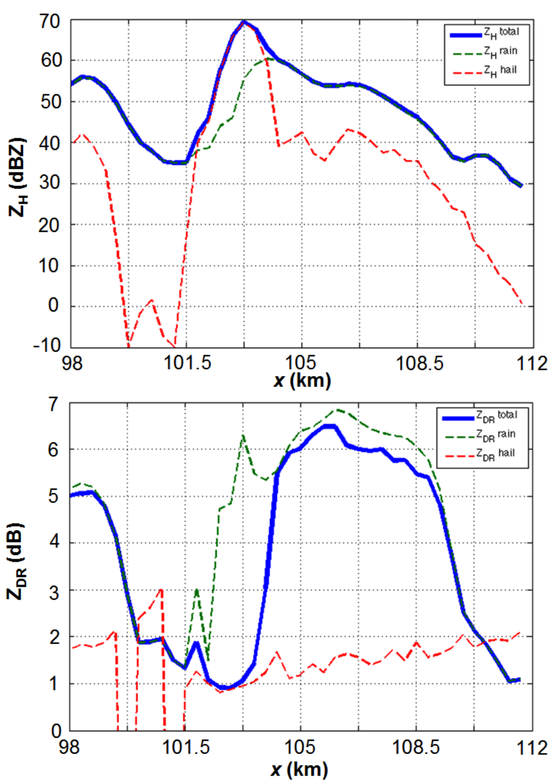

Fig. 9: Z_H (top panel) and Z_{DR} (bottom panel) through the hail core of the HUCM simulated storm. Total values are shown in blue; contributions from rain only (green dashed curve) and hail only (red dashed curve) are also shown.

4. OBSERVATIONS

Fig. 10 is a series of Z_H-Z_{DR} scattergrams from different elevation scans of the 1 June 2008 nontornadic supercell which produced hail up to the size of grapefruits. A special rapid-scanning strategy was implemented such that each elevation angle scan is separated by only 6 seconds, providing more validity in the interpretation of vertical structure in the storm. A detailed analysis of the storm and evolution of polarimetric radar signatures are provided in Kumjian et al. (2010b).

At low levels (3.5 km below the melting level), a majority of points have positive Z_{DR} and follow the expected values for rainfall in Oklahoma, as suggested by Cao et al. (2008). However, for larger Z_H values, there is a protrusion to negative Z_{DR} values (nearly -2 dB) likely associated with large and giant hail. Moving aloft, the Z_{DR} generally decreases towards 0 as the sampling volume approaches the melting layer. Above the melting layer, the data collapse around Z_{DR} ~ 0 dB, indicative of mainly ice hydrometeors. However, the points have a slight negative trend for higher Z_H values. By the highest elevation scan, where the center of the radar beam is at approximately 6.4 km above the melting level (AML), most of the large negative Z_{DR} values have disappeared. The largest hail in storms should be confined to the region of optimal growth between -10 and -20 ºC, according to Nelson (1983). Indeed, though the maximum Z_H does not change much between the 2.7 km AML and 6.4 km AML levels, a noticeable decrease in the number of negative Z_{DR} points does occur, consistent with the lack of any giant hail at the higher altitude. Note the good agreement between these observed data and those simulated in the HUCM (cf. Fig. 8).

The patterns revealed in the 1 June 2008 storm are observed in numerous other storm cases where large hail was reported (two are shown in Fig. 11a,b). For a case of a severe squall line in which no large hail is reported, the Z_H-Z_{DR} scatter pattern is confined closely to that expected of rainfall, with no protrusions to negative Z_{DR} (Fig. 11c). Fig. 11d is a schematic of subjectively-identified regions in Z_H-Z_{DR} space roughly corresponding to different precipitation types. Typical rainfall follows closely the Cao et al. (2008) line, whereas the “size sorting regime” indicates possible points where drop size distributions (DSDs) are skewed towards larger drops (i.e., high Z_{DR} and low Z_H). Such skewed DSDs indicate a sparse population of large raindrops and a relative deficit of smaller drops, which can be caused by vigorous size sorting in the presence of updrafts/downdrafts, strong rotation, and strong vertical wind shear (e.g., Kumjian and Ryzhkov 2008b, 2009). Small melting hail is identified in a large region that overlaps heavy rainfall significantly; note that the use of ρ_{HV} can reduce the uncertainty in the case of heavy rain versus heavy rain mixed with small hail at S band. The region for large hail is drawn conservatively, noting that large hail may exist for Z_H values less than 50 dBZ. This point is elaborated further in the next subsection.

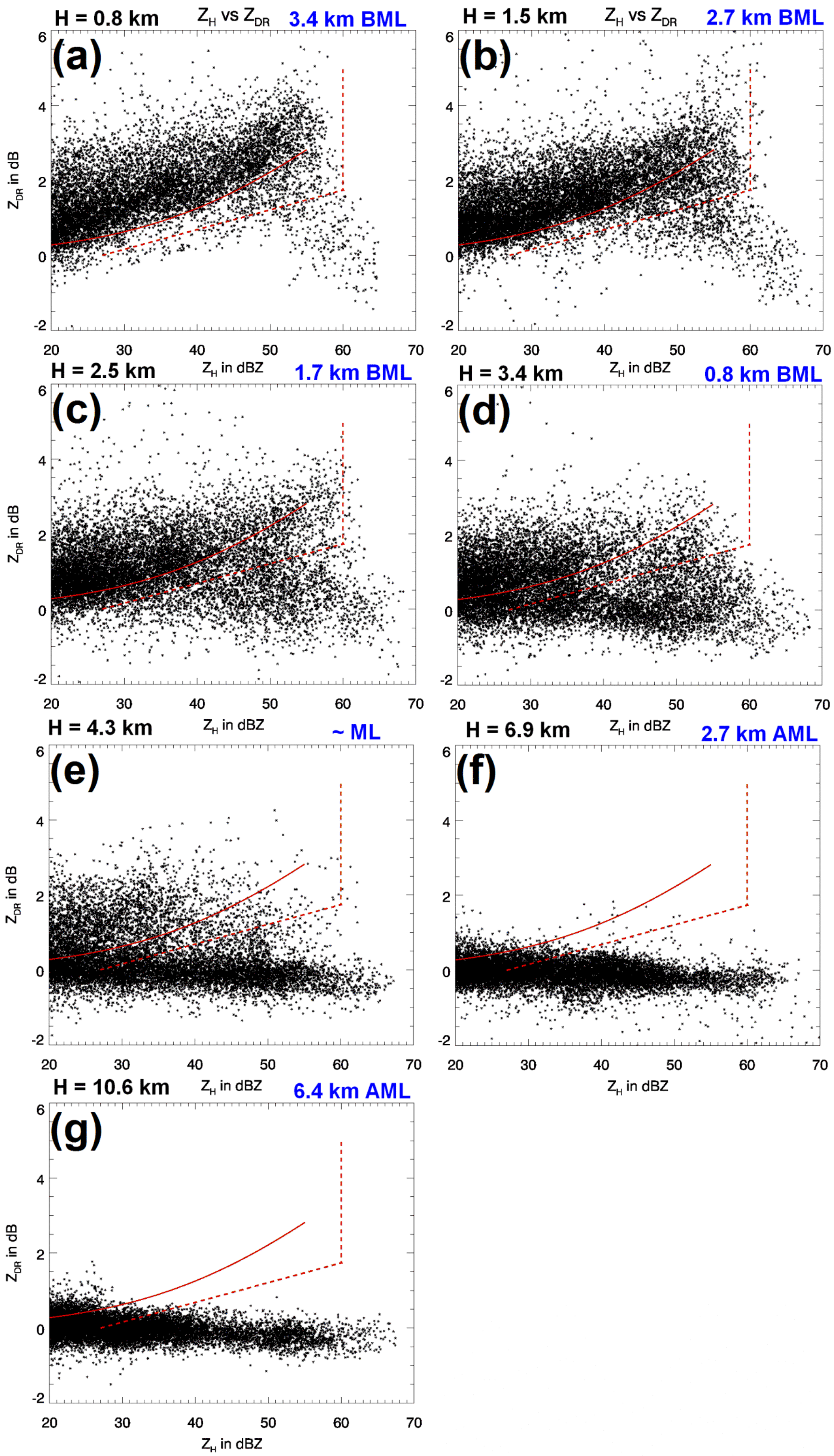

Fig. 10: Z_H-Z_{DR} scattergrams from different elevation scans of the 1 June 2008 nontornadic supercell storm. Approximate altitudes of the beamheights are indicated on the top left of each panel in black. Beamheights relative to the melting layer (4.2 km AGL) are indicated in blue font, with BML and AML referring to "below the melting level" and "above the melting level," respectively. The dotted red line is the Aydin et al. (1986) discrimination line, and the red solid curve is the Cao et al. (2008) line for rainfall in Oklahoma.

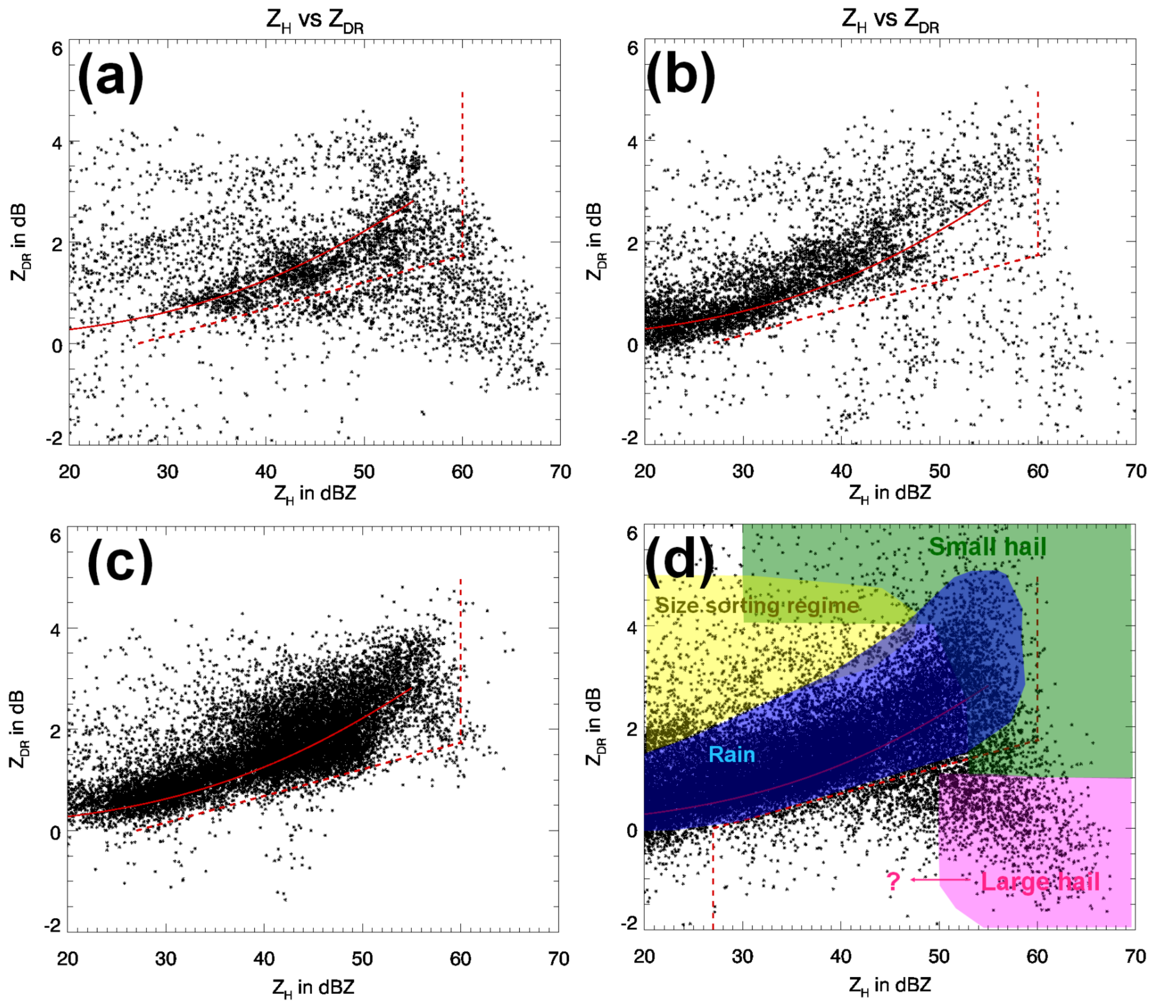

Fig. 11: As in Fig. 10, except for (a) 29 May 2004 supercell in which 5" hail was produced; (b) 30 March 2008 in which baseball-sized hail was produced; (c) 27 May 2008 severe MCS in which no large hail was reported. Panel (d) shows data from 1 June 2008 with subjectively-identified regions corresponding to rainfall (blue), small melting hail (green), large hail (pink), and a size-sorting regime (yellow).

4.1 Notes on Gigantic Hail

A common belief in the meteorology community is that larger hailstones produce larger Z_H, owing to the strong dependence on size ($Z_H \sim D^6$). However, Z_H is also dependent on particle concentration. Several recent cases reveal that anomalously large hail can fall in storms with maximum Z_H values that are not anomalously high. For example:

- 10 May 2010, Moore, OK: 5" hail, max $Z_H \sim 65$ dBZ
- 12 June 2010, Dumas, TX: 6.00", with max $Z_H \sim 65$ dBZ
- 23 July 2010, Vivian SD: 8.00", with max $Z_H < 70$ dBZ
- 15 Sept. 2010, Wichita, KS: 6"-7", with max $Z_H \sim 66$ dBZ.

The Z_H values listed above represent the *storm* maximum values at the lowest available scan. However, Payne et al. (2010) show that some of the largest hail on 10 May 2010 fell in regions with $Z_H < 45$ dBZ. Similarly, Picca and Ryzhkov (2010) find that the largest hailstones on the extremely damaging 16 May 2010 hailstorm did not fall in regions with the highest Z_H.

In fact, simple physical reasoning reveals that some of the largest hailstones are not expected to fall in the strongest core of storms. Supercells are known for their ability to produce some of the largest hailstones observed in nature, including all of the cases listed above. The presence of a mesocyclone allows hailstones to remain in favorable growth conditions within the updraft (e.g, Nelson 1983, Miller et al. 1988, 1990), where wet growth via the accretion of liquid water leads to rapid increases in hailstone mass. Because the largest hailstones grow within the updraft, one should expect such giant stones to fall in close proximity to the storm's updraft, as little horizontal advection will take place outside the updraft, owing to large particle fall speeds. Relative to low-level radar representations of supercells, the main updraft will be located approximately over the "inflow notch" that forms between the hook echo appendage and the forward flank echo. Thus, the largest hail should fall through or on the periphery of the updraft, at the edge of the low-level Z_H echoes. Indeed, a similar conceptual model was put forth by Browning (1964) as part of the "precipitation cascade."

In most cases, the number concentration of the largest hailstones is rather small: only a select few embryos injected into the updraft at optimal locations (e.g., Nelson 1983) can capitalize on the favorable growth conditions. Because of these low concentrations, it is possible that the *largest hailstones fall in regions of modest* Z_H. Observations by scientists in the VORTEX-2 field campaign indicated that the largest hailstones in some storms fell in very sparse concentrations in the absence of any other precipitation (Jeff Snyder, personal communication). The fact that giant hail in low concentrations causes only modest backscattered power underscores the utility of dual-polarization measurements to mitigate the ambiguity of Z_H measurements alone; whereas Z_H is dependent on concentration, Z_{DR} and ρ_{HV} are not. Thus, regions of storms close to the updraft (which can be inferred from the Z_{DR} column or updraft signatures) that are observed to have low ρ_{HV} and reduced Z_{DR} may contain large or giant hail, even without large Z_H.

5. SYNTHESIS OF RESULTS

Results from the theoretical models are consistent with those inferred from the observational data. Such agreement provides increased confidence in our ability to develop a preliminary set of rules that can be used to discriminate between large (> 1.0") and small (< 1.0") hail. It is desirable to build upon the existing polarimetric hydrometeor classification algorithm (HCA; see Park et al. 2009 for the latest version) that will be employed by the National Weather Service pending the nationwide upgrade of the WSR-88D network to polarimetric capabilities. Heinselman and Ryzhkov (2006) have demonstrated that the polarimetric HCA achieves 100% probability of detection of hail in addition to lower false alarm ratios than the conventional (single-polarization) hail detection algorithm (Witt et al. 1998). Because of the polarimetric HCA's skill in detecting areas of rain mixed with hail, the first step in discriminating hail size should be to identify regions likely containing hail. For each of the radar sampling volumes identified as containing a mixture of rain and hail, the height (above the ground) of the center of the resolution volume can be determined using the range and elevation angle. This beamheight should then be related to the height of the freezing level, which can be obtained using the WSR-88D melting layer detection algorithm (Giangrande et al. 2008), output from the RUC model (e.g., Benjamin et al. 2004), or operational rawinsondes. Depending on the difference between the beamheight (H) and the height of the freezing level (H_{FL}), the following preliminary set of rules can be used to recognized large hail:

$Z > 60$ dBZ if $H > H_{FL}$

$Z > 60$ dBZ and $Z_{DR} < 0.5$ dB if $0 < H_{FL} - H < 1$ km

$Z > 62$ dBZ and $Z_{DR} < 1.5$ dB if $1 < H_{FL} - H < 2$ km

$Z > 59$ dBZ and $Z_{DR} < 1.9$ dB if $2 < H_{FL} - H < 3$ km

$Z > 57$ dBZ and $Z_{DR} < 2.3$ dB if $H_{FL} - H > 3$ km

For illustration, we present the results of the polarimetric HCA output modified to distinguish between small and large hail (Fig. 12). The case is of the 16 May 2010 extreme hailstorm in Oklahoma City, which produced a large swath of damaging large and giant hail across the metro area. Maximum hail sizes exceeded 4.0" (10 cm). The case is analyzed in detail by Picca and Ryzhkov (2010, this conference). The HCA determines an expansive area of large (> 1.0") hail consistent with ground reports, depicted in pink. Note that the giant hail category (GH) is awaiting development and test of appropriate thresholds and was excluded from the algorithm for this example case.

A second case of multiple storm cells is tested next (Fig. 13). Several (but not all) of the cells in Fig. 13 are identified as having large hail. It is encouraging that the algorithm recognizes differences between the cells, although it is not a proof that it works well. There were numerous reports of large and giant hail about the time the data were collected; however, we do not claim that such reports constitute "proof" of the algorithm's accuracy. The HCA also misclassifies some ground clutter (near the radar) into rain, rain/hail, and even large hail. This would be avoided if ground clutter filters were applied to the data.

6. CONCLUDING REMARKS

The scattering and polarimetric radar characteristics of large hailstones have been presented. These properties are strongly dependent on hailstone size, axis ratio, fall behavior, and degree of melting. T-Matrix computations and theoretical explicit bin microphysics models of varying complexity have aided in quantifying these radar properties. The synthesis of the theoretical calculations and observations of hail-bearing storms has led to the development of a preliminary set of rules which, when incorporated into

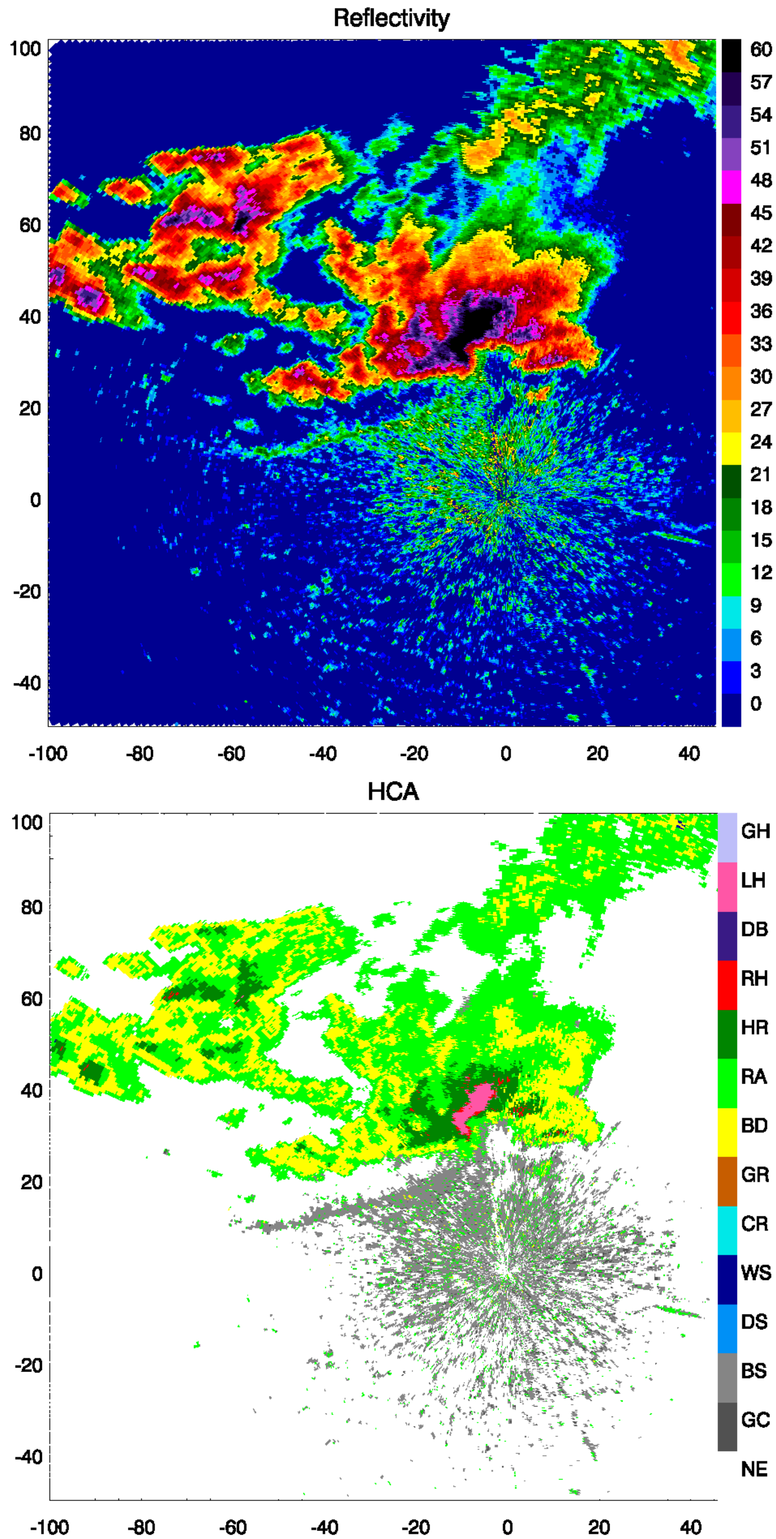

Fig. 12: *Example output from the polarimetric HCA modified to discriminate large and small hail. Categories included are: GC = ground clutter; BS = biological scatterers; DS = dry snow; WS = wet snow; CR = crystals; GR = graupel; BD = big drops; RA = rain; HR = heavy rain; RH = rain/hail mixture; DB = double category; LH = large hail; GH = giant hail (not included in the current algorithm). Data are from 16 May 2010 at 2059 UTC. The* Z_H *image is provided in the top panel for reference.*

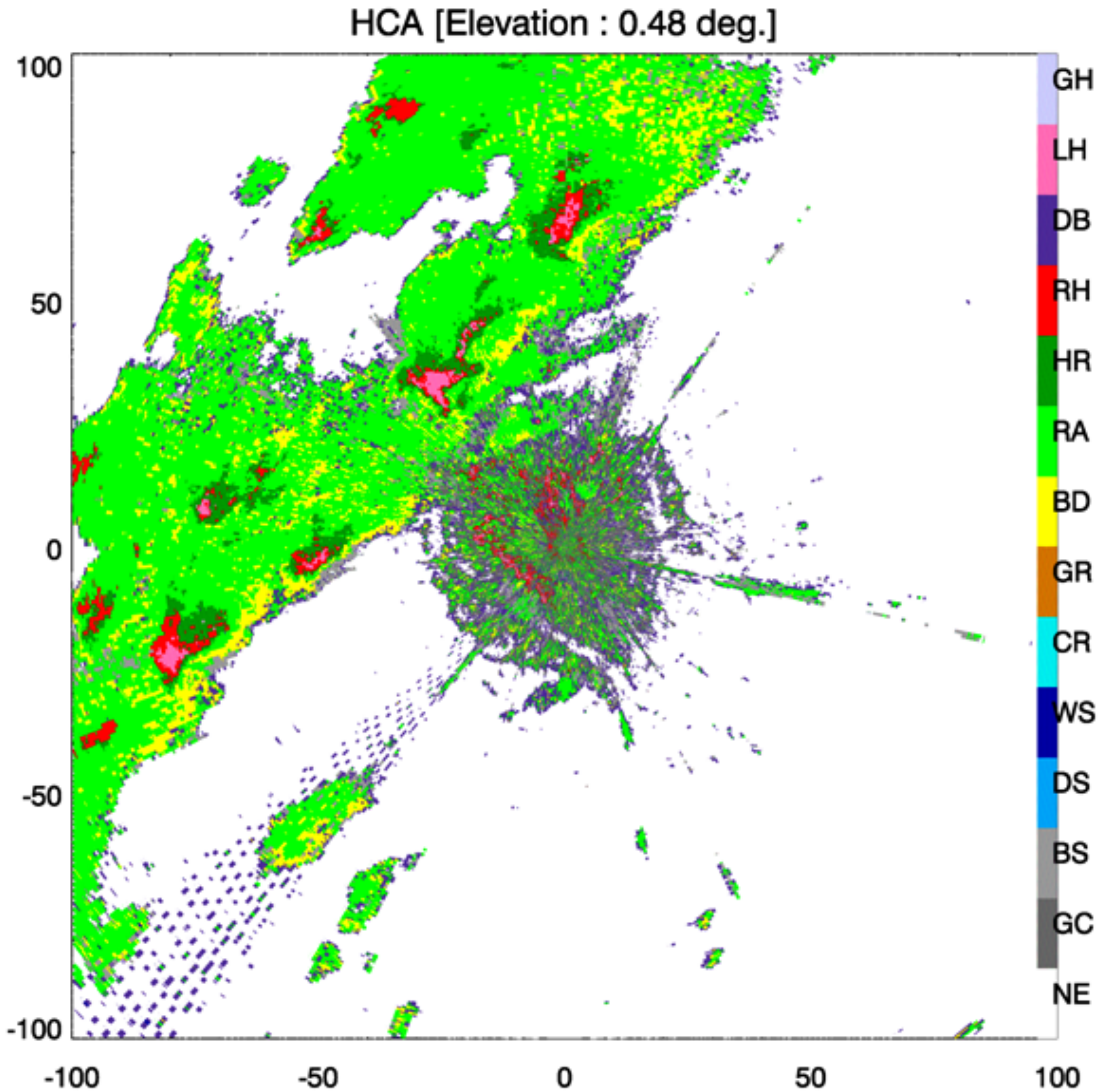

Fig. 13: As in Fig. 12, but the data are from 10 February 2010, at 0.48° elevation. The interference to the southwest of the radar is classified as "double category," as more than one category could not be reliably separated.

the existing NEXRAD hydrometeor classification algorithm, may be used to discriminate regions of large (> 1.0") and small (< 1.0") hail. The new discrimination algorithm has been tested on two cases of strong storms and has yielded encouraging results.

The main limitations of the theoretical approach are in uncertainty regarding fall behavior (i.e., rms width of the canting angle distribution) for particles of different sizes and the axis ratios of hailstones. Future observations with fully polarimetric radars may allow for measurements of the co-cross-polar correlation coefficients (ρ_{xh}, ρ_{xv}), which may provide information about the canting angle distribution width (e.g., Ryzhkov 2001). Concerning the new discrimination algorithm, testing on more cases in which substantial ground truth exists may aid in the accuracy of the algorithm as well as increase confidence in its reliability. Planned special observations of future hail storms will provide information not only on maximum hail size, but on the shapes, distributions of sizes, and other hydrometeors present. Future versions of the algorithm will also incorporate a "giant hail" category, which presently awaits more detailed analysis of observations and theoretical computations.

7. ACKNOWLEDGMENTS

This work is partly funded by NOAA/University of Oklahoma Cooperative Agreement NA17RJ1227 under the U.S. Dept. of Commerce. Additional support comes from an agreement with the Massachusetts Institute of Technology Lincoln Laboratory.

8. REFERENCES

Aydin, K., T.A. Seliga, and V.Balaji, 1986: Remote sensing of hail with a dual linear polarization radar. J. Climate Appl. Meteor., **25,** 1475-1484.

Aydin, K., and Y. Zhao, 1990: A computational study of polarimetric radar observables in hail. *IEEE Trans. Geosci. Remote Sens.,* **28**, 412-422.

Balakrishnan, N. and D.S. Zrnic, 1990: Use of polarization to characterize precipitation and discriminate large hail. *J. Atmos. Sci.*, **47**, 1525-1540.

Benjamin, S.G., D. Dévényi, S.S. Weygandt, K.J. Brundage, J.M. Brown, G.A. Grell, D. Kim, B.E. Schwartz, T.G. Smirnova, and T.L. Smith, 2004: An hourly assimilation-forecast cycle: The RUC. *Mon. Wea. Rev.*, **132**, 495-518.

Böhm, J.P., 1991: Review of flow characteristics and kinematics of hydrometeors in free fall. *Atmos. Res.*, **26**, 285-302.

Browning, K.A., 1964: Airflow and precipitation trajectories within severe local storms which travel to the right of the winds. *J. Atmos. Sci.*, **21**, 634-639.

Cao, Q., G. Zhang, E. Brandes, T. Schuur, A.V. Ryzhkov, and K. Ikeda, 2008: Analysis of video disdrometer and polarimetric radar data to characterize rain microphysics in Oklahoma. *J. Appl. Meteor. and Climatology*, **47**, 2238-2255.

Clabo, D., P. Smith, and A. Detwiler, 2009: Polarimetric radar signatures of hydrometeors observed within mature convective storms. *Extended Abstracts*, 34th Conf. on Radar Meteorology, Amer. Meteor. Soc., Williamsburg, VA, P13.5. [Available online at http://ams.confex.com/ams/pdfpapers/155110.pdf].

Depue, T., P Kennedy, and S. Rutledge, 2007: Performance of the hail differential reflectivity (HDR) polarimetric hail indicator. *J. Appl. Meteor. Climatology*, **46**, 1290-1301.

Giangrande, S.E., J.M. Krause, and A.V. Ryzhkov, 2008: Automatic designation of the melting layer with a polarimetric prototype of the WSR-88D radar. *J. Appl. Meteor. and Climatology*, **47**, 1354-1364.

Heinselman, P. and A. V. Ryzhkov, 2006: Validation of polarimetric hail detection. *Wea. Forecasting*, **21**, 839-850.

Khain, A., A. Pokrovsky, M. Pinsky, A. Seifert, and V. Phillips, 2004: Effects of atmospheric aerosols on deep convective clouds as seen from simulations using a spectral microphysics mixed-phase cumulus cloud model. Part I: Model description. *J. Atmos. Sci.*, **61**, 2963-2982.

Knight, C.A., and N.C. Knight, 1970: The falling behavior of hailstones. *J. Atmos. Sci.*, **27**, 672-681.

Knight, N.A., 1986: Hailstone shape factor and its relation to radar interpretation of hail. *J. Appl. Meteor.*, **25**, 1956-1958.

Kry, P.R., and R. List, 1974: Angular motions of freely falling spheroidal hailstone models. *Phys. Fluids*, **17**, 1093-1102.

Kumjian, M.R. and A.V. Ryzhkov, 2008: Interpretation of polarimetric signatures in supercell storms using explicit microphysical modeling. Extended Abstracts, *5th European Conf. on Radar Meteor.*, Helsinki, Finland, P7.2. [Available online at http://erad2008.fmi.fi/proceedings/extended/erad2008-0065-extended.pdf]

Kumjian, M.R. and A.V. Ryzhkov, 2008b: Microphysical size sorting revealed by dual-polarization Doppler radar. *Extended Abstracts*, 88th Annual AMS Meeting, New Orleans, Amer., Meteor. Soc., P2.13. [Available online at http://ams.confex.com/ams/pdfpapers/133439.pdf]

Kumjian, M.R. and A.V. Ryzhkov, 2009: Storm-relative helicity revealed from polarimetric radar observations. *J. Atmos. Sci*., **66**, 667–685.

Kumjian, M.R., J.C. Picca, S. Ganson, A.V. Ryzhkov, and D.S. Zrnic, 2010a: Three body scattering signatures in polarimetric radar data. *NOAA/NSSL Report*, 12 pp. Available online at: http://publications.nssl.noaa.gov/wsr88d_reports/FINAL_TBSS.doc

Kumjian, M.R., A.V. Ryzhkov, V.M. Melnikov, and T.J. Schuur, 2010b: Rapid-scan super-resolution observations of a cyclic supercell with a dual-polarization WSR-88D. *Mon. Wea. Rev.*, **138**, 3762-3786.

Liu, H., and V. Chandrasekar, 2000: Classification of hydrometeors based on polarimetric radar measurements: Development of fuzzy logic and neuro-fuzzy systems, and in situ verification. *J. Atmos. Oceanic Technol.*, **17**, 140-164.

Lim, S., V. Chandrasekar, and V.N. Bringi, 2005: Hydrometeor classification system using dual-polarization radar measurements: model improvements and *in situ* verification. *IEEE Transactions on Geoscience and Remote Sensing*, **43**, 792-801.

Milbrandt, J.A. and M.K. Yau, 2006: A multimoment bulk microphysics parameterization. Part III: Control simulation of a hailstorm. *J. Atmos. Sci.*, **63**, 3114-3136.

Miller, L.J., J.D. Tuttle, and C.A. Knight, 1988: Airflow and hail growth in a severe northern High Plains supercell. *J. Atmos. Sci.*, **45**, 736-762.

Miller, L.J., K.D. Tuttle, and G.B. Foote, 1990: Precipitation production in a large Montana hailstorm: Airflow and particle growth trajectories. *J. Atmos. Sci.*, **47**, 1619-1646.

Nelson, S.P., 1983: The influence of storm flow structure on hail growth. *J. Atmos. Sci.*, **40**, 1965-1983.

Park, H.-S., A. Ryzhkov, D. Zrnic, and K.E Kim, 2009: The hydrometeor classification algorithm for polarimetric WSR-88D. Description and application to an MCS. *Wea. Forecasting*, **24**, 730-748.

Payne, C.D., C.A. Van Den Broeke, L.R. Lemon, and P.T. Schlatter, 2010: Polarimetric radar characteristics of a supercell hailstorm on 10 May 2010 in central Oklahoma. *Extended Abstracts,* 25th Conf. on Severe Local Storms, Denver, CO, Amer. Meteor. Soc., P8.7.

Picca, J.C., and A.V. Ryzhkov, 2010: A multiple-wavelength polarimetric analysis of the 16 May 2010 Oklahoma City extreme hailstorm. *Extended Abstracts*, 25th Conf. on Severe Local Storms, Denver CO, Amer. Meteor. Soc., P8.6.

Rasmussen, R.M. and A.J. Heymsfield, 1987: Melting and shedding of graupel and hail. Part I: Model physics. *J. Atmos. Sci.*, **44**, 2754-2763.

Ryzhkov, A.V., 2001: Interpretation of polarimetric radar covariance matrix for meteorological scatterers: Theoretical analysis. *J. Atmos. Oceanic Technol.* **18**, 315-328.

Ryzhkov, A.V., S.M. Ganson, A. Khain, M. Pinsky, and A. Pokrovsky, 2009: Polarimetric characteristics of melting hail at S and C bands. *Extended Abstracts*, 34th Conf. on Radar Meteorology, Amer. Meteor. Soc., Williamsburg, VA, 4A.6.

Ryzhkov, A.V., M. Pinsky, A. Pokrovsky, and A. Khain, 2010: Polarimetric radar observation operator for a cloud model with spectral microphysics. *J. Appl. Meteor.*, **in press.**

Straka, J.M., D.S. Zrnic, and A.V. Ryzhkov, 2000: Bulk hydrometeor classification and quantification using polarimetric radar data: Synthesis of relations. *J. Appl. Meteor.*, **39**, 1341-1272.

Wakimoto, R.M., and V.N. Bringi, 1988: Dual-polarization observations of microbursts associated with intense convection: The 20 July storm during the MIST Project. *Mon. Wea. Rev.*, **116**, 1521-1539.

Witt, A., M.D. Eilts, G.J. Stumpf, J.T. Johnson, E. D. Mitchell, and K.W. Thomas, 1998: An enhanced hail detection algorithm of the WSR-88D. *Weather and Forecasting*, **13**, 286-303.